ACS Catalysis

Letter

pubs.acs.org/acscatalysis

Water-Mediated Mars–Van Krevelen Mechanism for CO Oxidation on Ceria-Supported Single-Atom Pt_1 Catalyst

Chunlei Wang,[†,∥] Xiang-Kui Gu,[‡,∥] Huan Yan,[†] Yue Lin,[†] Junjie Li,[†] Dandan Liu,[†] Wei-Xue Li,*[,†] and Junling Lu*[,†]

[†]Department of Chemical Physics, iChem, Hefei National Laboratory for Physical Sciences at the Microscale, CAS Key Laboratory of Materials for Energy Conversion, CAS Center for Excellence in Nanoscience, University of Science and Technology of China, Hefei, Anhui 230026 P. R. China

[‡]School of Chemical Engineering, Purdue University, West Lafayette, Indiana 47907, United States

Supporting Information

ABSTRACT: In water-promoted CO oxidation, water was thought not to directly participate in CO_2 production. Here we report that via a water-mediated Mars–van Krevelen (MvK) mechanism, water can directly contribute to about 50% of CO_2 production on a single-atom Pt_1/CeO_2 catalyst. The origin is the facile reaction of CO with the hydroxyl from dissociated water to yield the carboxyl intermediate, which dehydrogenates subsequently with the help of a lattice hydroxyl to generate CO_2 and water. The water-mediated MvK type reaction found here provides new insights in the promotion role of water in heterogeneous catalysis.

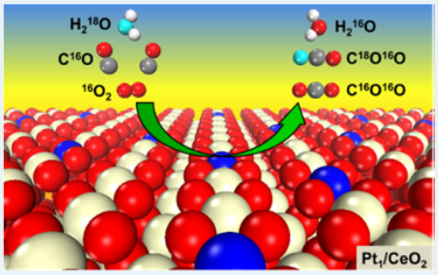

KEYWORDS: *CO oxidation, single atom catalyst, Pt_1/CeO_2, water promotion, Mars–van Krevelen*

Water, the most abundant molecule in our planet and widely present under ambient conditions, plays important roles in a wide range of chemical reactions in heterogeneous catalysis. It can be a reaction media in liquid-phase reactions[1] or a reactant in water gas shift (WGS),[2] hydrolysis,[3] and steam reforming.[4,5] Moreover, water can be a promoter or cocatalyst to dramatically increase catalytic activity,[6−14] or even an inhibitor to quickly deactivate a catalyst.[15−17] Revealing the corresponding reaction mechanism and identification of the active sites are vital for rational design of catalysts. Water-promoted CO oxidation over supported gold nanoparticles has been studied extensively. It was proposed that water enhanced the reaction by promoting the decomposition of the intermediates.[7,18] Alternatively, water was also suggested to stabilize the adsorption of oxygen molecules by formation of a hydrogen bond,[19−22] or to assist the activation of oxygen molecules by formation of hydroperoxyl.[23] In these studies, neither water nor lattice oxygen of supports directly participates in the final CO_2 production.[24,25] The reaction followed the water-mediated Langmuir–Hinshelwood (L–H) mechanism. Despite the great progress and valuable insights obtained from these investigations, the very nature of water promotion in catalysis remains elusive, complicated further by the presence of numerous distinct sites in corner, edge, facet, and metal–support perimeter of the supported metal nanoparticles.

We report here a great promotion of water in CO oxidation with direct participation in the final CO_2 production via the water-mediated Mars–van Krevelen (MvK) mechanism on a single-atom Pt_1/CeO_2 catalyst. The Pt_1/CeO_2 catalyst with uniform active sites and maximized atomic efficiency was prepared using the atomic layer deposition (ALD) technique.[26−28] Compared to the minimal catalytic activity of Pt_1/CeO_2 below 100 °C under dry conditions, remarkably, 100% CO conversion was found at 98 °C in the presence of water. Density functional theory (DFT) calculations found that water promotion comes from assisting in reaction of CO with the hydroxyl from dissociated water to yield a carboxyl intermediate, and this intermediate subsequently decomposes with the help of a lattice hydroxyl to generate CO_2 and water. Actually, water contributed to about 50% of the final CO_2 production but with zero net consumption, as indicated by DFT calculations and proved by subsequent isotope-labeling experiments. This is in sharp contrast to the reported water-mediated L–H mechanism.[24,25] The water-mediated MvK mechanism found here provides a new scenario for the promotion of water in heterogeneous catalysis.

We have demonstrated that fabrication of single-atom metal catalysts using ALD is possible by careful control over the type and density of nucleation sites and the deposition temperature.[27] Here a single-atom Pt_1/CeO_2 catalyst with a loading of 0.22% was first synthesized using ALD by exposing (methylcyclopentadienyl)-trimethylplatinum ($MeCpPtMe_3$) at 150 °C followed by calcination at 200 °C in 10% O_2 in Ar to remove the ligands. Aberration-corrected high-angle annular dark-field scanning transmission electron microscopy

Received: September 20, 2016
Revised: November 14, 2016
Published: December 21, 2016

DOI: 10.1021/acscatal.6b02685
ACS Catal. 2017, 7, 887−891

(HAADF-STEM) images at different locations clearly revealed that individual Pt atoms (marked by the white circles) were uniformly dispersed on the CeO_2 support without presence of any Pt clusters and nanoparticles (Figures 1a–d, S1 and S2).

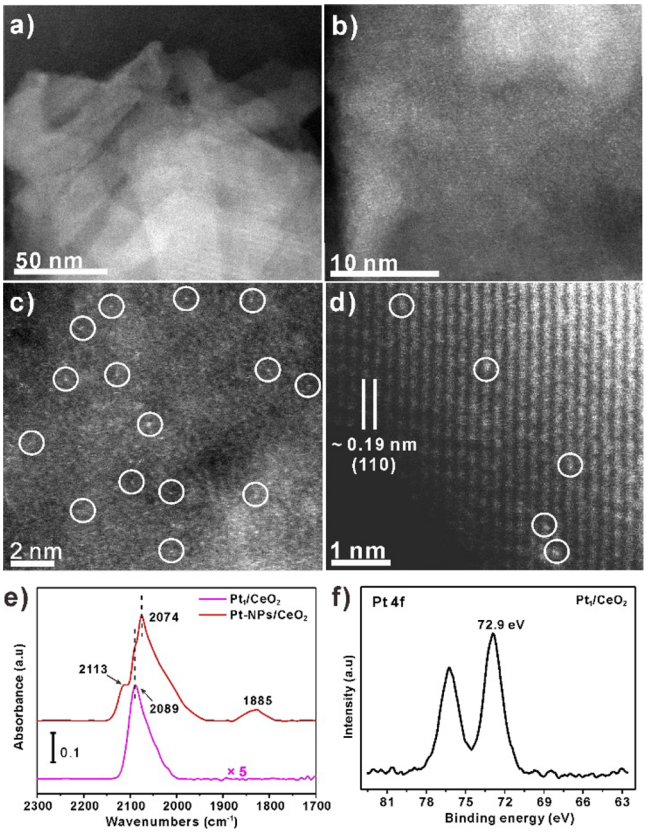

Figure 1. Representative HAADF-STEM images of the resulting Pt_1/CeO_2 catalyst at (a and b) low and (c and d) high magnifications. A portion of the atomically dispersed Pt atoms in images (c and d) are highlighted by the white circles. (e) DRIFTS of CO chemisorption on Pt_1/CeO_2 and Pt-NPs/CeO_2. (f) XPS spectrum of the Pt_1/CeO_2 sample in the Pt 4f region.

Further analyzing the high-resolution STEM images at different locations revealed that the isolated Pt atoms are mainly located on the Ce rows of CeO_2(110) facet (Figure 1d) and on the CeO_2(100) facet (Figure S3). However, it was surprising that no obvious Pt atoms were found on CeO_2(111) facet (Figure S4). Consistent with the STEM observations, X-ray diffraction (XRD) measurements (Figure S5) did not reveal any Pt-related diffraction peaks on Pt_1/CeO_2, implying the absence of large Pt nanoparticles.

Infrared spectroscopy using CO as the probe molecule is a fast and convenient characterization method to directly differentiate single atoms from nanoparticles.[29,30] Here diffuse reflectance infrared Fourier transform spectroscopy (DRIFTS) CO chemisorption measurements were performed on the single-atom Pt_1/CeO_2 catalyst and a sample of CeO_2-supported Pt nanoparticles (designated as Pt-NPs/CeO_2, seen in Figure S6) for comparison (Figure 1e). On Pt-NPs/CeO_2, the peaks at 2074 and 1835 cm^{-1} are assigned to the linear- and bridge-bonded CO on Pt, respectively.[29,30] The shoulder at 2113 cm^{-1} was assigned to linear CO on oxidized Pt particles.[31] Thus, the bridge-bonded CO at 1835 cm^{-1} can be a signature of Pt atom ensembles of Pt clusters or nanoparticles.[30] On Pt_1/CeO_2, only a peak at 2089 cm^{-1} was observed, which is very close to the value on isolated Pt atoms reported in literature.[30] A blue shift of 15 cm^{-1} compared to the linear CO on Pt nanoparticles (2074 cm^{-1}) is attributed to CO adsorbed on the positively charged Pt single atoms. Indeed, XPS measurements showed the Pt $4f_{7/2}$ binding energy was 72.9 eV on Pt_1/CeO_2 (Figure 1f), indicating that the oxidation state of the Pt single atoms is between Pt^{2+} and Pt^{4+}, according to the literature.[32,33] In addition, the absence of bridge-bonded CO suggests that either Pt clusters or nanoparticles were not present on Pt_1/CeO_2.[30]

Next, we evaluated the single-atom Pt_1/CeO_2 catalyst in CO oxidation with/without the presence of water. Under dry conditions (designated as Pt_1/CeO_2), Pt_1/CeO_2 showed barely any catalytic activity below 100 °C, and 100% CO conversion was obtained at about 160 °C (Figure 2a). With the presence of

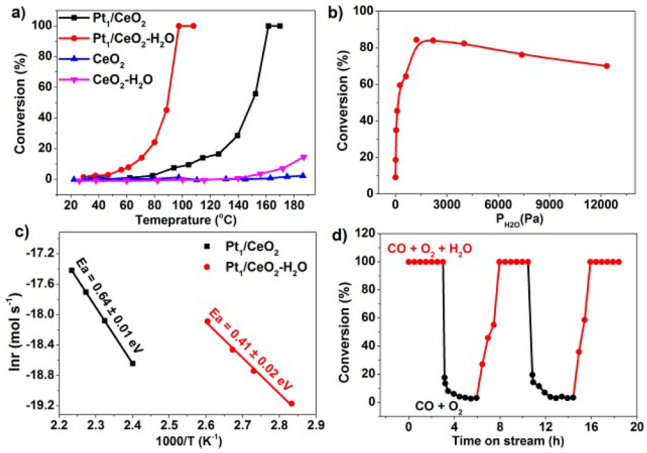

Figure 2. (a) Catalytic activity of the single-atom Pt_1/CeO_2 catalyst and the blank CeO_2 support in CO oxidation with/without the presence of water. (b) Changes of CO conversion at 96 °C as a function of water partial pressure. (c) Arrhenius plots for CO oxidation on Pt_1/CeO_2 with/without the presence of water. (d) Activity changes at 98 °C by switching on and off water. Reaction conditions: 1% CO and 20% O_2 in Ar; water partial pressure 4000 Pa; total flow rate 30 mL/min.

water (designated as Pt_1/CeO_2–H_2O), the activity was remarkably improved by achieving the 100% CO conversion at 98 °C. As a comparison, the blank CeO_2 support showed barely any activity at below 160 °C in CO oxidation with/without the presence of water. Varying water partial pressure from ~13 to 12 300 Pa (Figure 2b), we found that the activity sharply increased below 1200 Pa and reached the maximum at around 1200–2200 Pa; then it gradually decreased at higher water partial pressures, in line with literature.[8] Such water promotion effect was also demonstrated by the DRIFTS measurements of the evolution of prechemisorbed CO on Pt_1/CeO_2 during sequential O_2 and O_2 + H_2O purge at 50 °C (Figure S7), wherein the intensity of chemisorbed CO on Pt_1/CeO_2 remained intact during O_2 purge, similar to the recent work by Stair et al.,[29] but quickly decreased during the O_2 + H_2O purge. The Arrhenius plots in Figure 2c illustrate that the presence of water significantly reduced the apparent activation barrier from 0.64 ± 0.01 to 0.41 ± 0.02 eV. Nonetheless, we noticed that the WGS reaction did not occur at below 200 °C (Figure S8), consistent with literature.[2]

The stability, in particular at elevated temperatures, is crucial for single-atom catalysts.[27,34–36] Here we examined the stability

DOI: 10.1021/acscatal.6b02685
ACS Catal. 2017, 7, 887–891

of the single-atom Pt_1/CeO_2 catalyst at 98 °C by switching on and off water (Figure 2d, also see another recycling stability test in Figure S9). The CO conversion quickly declined from 100% to ~8% in ~30 min once the humid reaction gas (water pressure: 4000 Pa) was switched to dry gas. Next, switching back to the humidity fully recovered the catalyst activity. Such declination and recovery of the catalyst activity by switching on and off water clearly demonstrates the water promotion effect and suggests that the single-atom Pt_1/CeO_2 catalyst was rather stable under the current conditions. A long-term stability test at 92 °C in the H_2O-promoted CO oxidation also illustrated the activity was virtually preserved after 96 h (Figure S10). HAADF-STEM measurements on the used catalyst illustrated that nearly all isolated Pt atoms survived after the long-term stability test, and only a few Pt clusters were observed (Figures S11 and S12).

DFT calculations were performed to shed light on the CO oxidation over Pt_1/CeO_2 with/without the presence of water. Considering the observation by STEM, we first focused on the $CeO_2(110)$ facet. After optimizing various structures (Figure S13), we found that single Pt atom substitution in the surface Ce vacancy is most stable (noted as $Pt_1/CeO_2(110)$), where the positively charged Pt atom is stabilized by the lattice oxygen via six Pt−O bonds (Figure 3i). The calculated vibrational frequency of CO on top of the substituted Pt atom is 2076 cm^{-1} (Figure S14), a blue shift of 17 cm^{-1} compared to the calculated frequency of 2059 cm^{-1} for linear CO on Pt(111), which is consistent very well with our experimental blue-shift value of 15 cm^{-1} between Pt_1/CeO_2 and Pt-NPs/CeO_2 (Figure 1d). This blue shift also agrees well with literature,[31] where CO

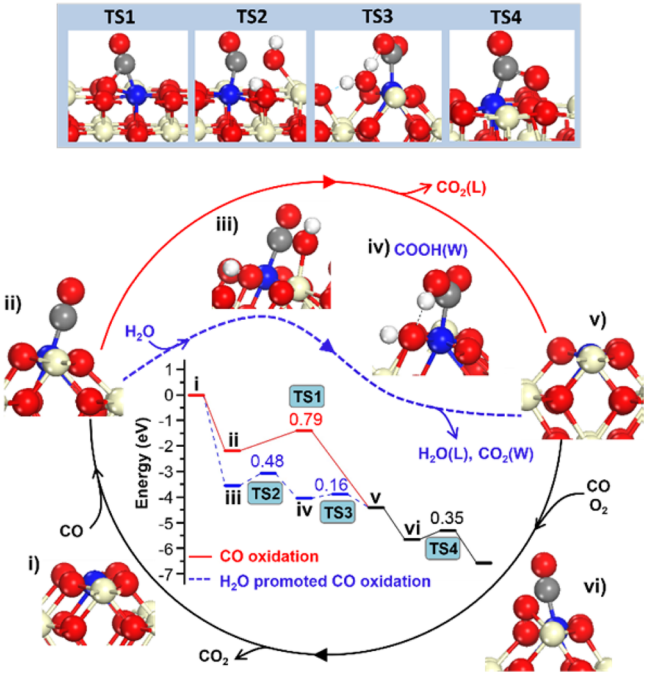

Figure 3. Proposed reaction pathways for CO direct oxidation and H_2O-promoted CO oxidation on $Pt_1/CeO_2(110)$. Here the structures of intermediates and transition states (TS) of the key elementary steps are present. The inset in the reaction cycles shows the calculated energy profile in eV. After one catalytic cycle in both cases, the catalyst is recovered and releases two CO_2 molecules. The yellow, blue, red, gray, and white spheres represent Ce, Pt, O, C, and H atoms, respectively.

on $Pt^{\delta+}$ has a higher vibrational frequency than on Pt^0. The calculated Bader charge of Pt_1 in $Pt_1/CeO_2(110)$ is +1.38 |e|. Compared with the calculated values of +0.95 |e| and +1.62 |e| for Pt in bulk PtO and PtO_2, the oxidation state of Pt_1 is closer to Pt^{4+}, which is again consistent well with our XPS results shown in Figure 1f. Whereas for $CeO_2(100)$ facet, single Pt atom substitution in the surface Ce vacancy was adopted (Figure S13), and various structural models were tested (Figure S14). Unfortunately, either there was no stable configuration for CO linear adsorption at Pt_1−top found, or the calculated CO stretching frequencies fall in the range far below the measured values. The $CeO_2(100)$ facet is excluded therefore, although isolated Pt atoms on $CeO_2(100)$ facet are observed by STEM (Figure S3).

In the absence of water, CO adsorbs firmly on Pt_1-top with a binding energy of −2.18 eV (Figure 3ii). Compared to CO adsorption at the step edge of the vicinal Pt(211) surface, the binding strength increases by 0.20 eV. To rationalize this, we note that Pt_1 is cationic and electron deficient. As a result, the donation of CO 5σ orbital toward Pt_1 is enhanced, whereas the back-donation of Pt_1 toward CO 2π* is weakened. Indeed, compared to an overall electron transfer of 0.18 *e* from the Pt(211) substrate to CO, it decreases to 0.06 *e* only on $Pt_1/CeO_2(110)$. On the other hand, the binding strength of CO on Pt_1-top is much stronger than the binding of oxygen molecule (−0.86 eV) at the same site. This implies that CO will dominate the Pt_1-site during CO oxidation. The adsorbed CO can react with the surface lattice oxygen O(L) coordinated with the Pt_1 atom to form CO_2(L) (Figure 3, TS1). The calculated barrier is 0.79 eV, exothermic by 2.22 eV (see inset in Figure 3). After desorption of CO_2(L) formed, there is one lattice oxygen vacancy V_O left (Figure 3, v). The surface can coadsorb one oxygen molecule at V_O and one CO at Pt_1-top (Figure 3, vi). The differential binding energy of oxygen molecule at V_O is −1.06 eV, and the oxygen molecule is nearly perpendicular to the surface. Compared to O_2 in gas phase, the corresponding O−O bond length was elongated by 0.2 Å. This indicates that the oxygen molecule at V_O is activated, which is understandable considering the great redox activity of ceria. Indeed, the high-lying oxygen of oxygen molecule easily reacts with CO at Pt_1-top to form CO_2 with a barrier of 0.35 eV and exothermicity of 0.92 eV (Figure 3, TS4). The catalytic cycle is close after desorption of CO_2. The reaction scenario revealed follows the MvK mechanism.[37,38]

To evaluate the role of water in CO oxidation, we first note that H_2O can adsorb molecularly at Pt_1-top with a binding energy of −1.62 eV. However, CO binding strength at the same site remains 0.56 eV stronger. This means that CO is still dominating the Pt_1 sites even in the presence of water. This rationalizes well the experimental finding; that is, CO chemisorption on water-pretreated Pt_1/CeO_2 was identical to CO on the untreated sample (Figure S15). Alternatively, water can molecularly adsorb on CeO_2 with a binding energy of −0.96 eV, similar to the previously reported value of −0.89 eV.[39] The molecular water can easily dissociate to a hydroxyl OH(W) at Ce-top and a lattice hydroxyl OH(L) nearby (Figure 3, iii). This process is exothermic by 1.36 eV and nearly barrierless, consistent with the experimental finding of a facile water partial dissociation on CeO_2.[39,40] The hydroxyl at Ce-top readily associates with CO at Pt_1-top to form a carboxyl COOH(W) intermediate (Figure 3, iv) with exothermicity of 0.49 eV. The corresponding barrier is 0.48 eV (see inset in Figure 3), which is much lower than that of 1.02 eV in the

DOI: 10.1021/acscatal.6b02685
ACS Catal. 2017, 7, 887−891

alternative pathway, namely, CO association with the lattice hydroxyl (Figure S16). Dehydrogenation of the carboxyl intermediate with the help of a lattice hydroxyl nearby to generate CO_2(W) and H_2O(L) is very fast with a barrier of 0.16 eV only (Figure 3, TS3). Subsequent desorption of CO_2(W) and H_2O(L) into gas phase is exothermic by 0.37 eV (Figure 3, v). Similar to the above, the catalyst surface with an oxygen vacancy left can coadsorb O_2 and CO (Figure 3, vi) to produce the second CO_2 by passing through a small barrier of 0.35 eV. The surface is recovered, and the catalytic cycle in the presence of water is closed. We noted that the surface might be hydroxylated during the water assisted CO oxidation process. However, the coverage of surface hydroxyls was found to have less significant influence on the above reaction mechanism (Figure S17).

An interesting discovery from calculation is the direct participation of water in CO oxidation; that is, half the amount of CO_2 product comes from the association between CO and the hydroxyl from dissociated water at Ce-top. Subsequently, the H abstraction from the carboxyl intermediate toward the lattice hydroxyl regenerates water. As a result, there is no water consumption in the overall process. Compared to the desorption of H_2O(L) formed, its dehydrogenation to produce H_2 is highly endothermic by 4.02 eV. This implies that WGS on Pt_1/CeO_2(110) cannot take place, in good agreement with our experimental result where no WGS activity was observed below 200 °C (Figure S8).

The above calculations show that the rate-limiting step (RLS) in the absence of water is the CO reaction toward the surface lattice oxygen with a barrier of 0.79 eV. However, the RLS in the presence of water becomes the CO reaction toward the hydroxyl group from dissociated water at Ce−top with barrier of 0.48 eV. Water promotion on CO oxidation is evident by lowering the RLS barrier by 0.31 eV, which is close to the decrease of the measured apparent barrier for CO oxidation by 0.23 eV (Figure 2c). The water mediation in MvK with a lower overall barrier is therefore the main reason for the higher activity of Pt_1/CeO_2 in the presence of water. It is worth noting that previous calculation suggested that on bare CeO_2 water inhabits the CO oxidation reaction,[41] whereas the present work shows that in the presence of Pt_1, water can significantly promote the CO oxidation reaction.

To examine the suggested catalytic reaction pathways above in the H_2O-promoted CO oxidation, $H_2{}^{18}O$ isotope-labeling experiments were performed, where the pulses of the reaction products were recorded by mass spectroscopy. Indeed, comparing to the CO oxidation without water (Figure 4a), nearly half amount of CO_2 in the form of $C^{16}O^{18}O$ was detected in the $H_2{}^{18}O$-promoted CO oxidation at the reaction steady stage (Figure 4b). In addition, we also observed a significant amount of $H_2{}^{16}O$ formation, compared to the $H_2{}^{16}O$ background as shown in Figure S18, which is not surprising because a $H_2{}^{16}O$ molecule is released by consuming one lattice ^{16}O along with the first CO_2(W) formation according to the calculated catalytic cycle with water (Figure 3, TS3). As shown in Figure 4c, $C^{16}O^{18}O$ could be also formed at room temperature but with a significantly higher $C^{16}O_2$ to $C^{16}O^{18}O$ ratio of 16.3. Increasing the reaction temperature, the $C^{16}O_2$ to $C^{16}O^{18}O$ ratio quickly decreased and reached stable regime of near 1:1 at near 90 to 105 °C. At lower temperatures, the formed $H_2{}^{16}O$ molecules readsorb on the catalyst surface and participate in the reaction, thereby giving the higher $C^{16}O_2$ to $C^{16}O^{18}O$ ratio. Therefore, the $H_2{}^{18}O$ isotope-labeling experiments provide a conclusive proof on the proposed mechanism from DFT calculation.

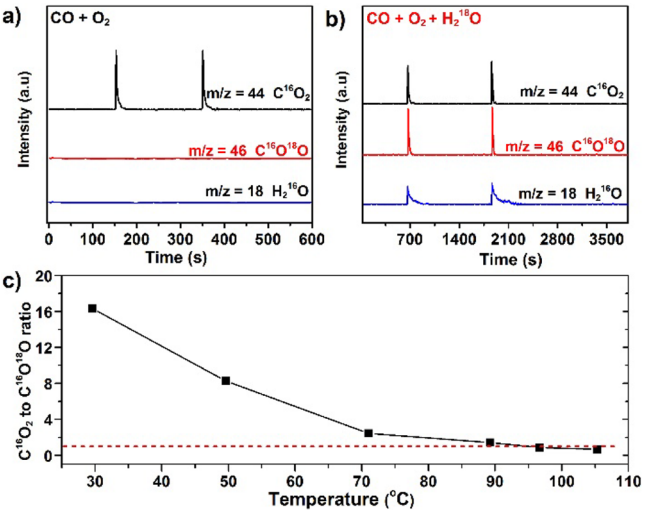

Figure 4. Time-dependent mass spectra of the pulses of the $C^{16}O_2$, $C^{16}O^{18}O$, and $H_2{}^{16}O$ in the direct CO oxidation (a) and the $H_2{}^{18}O$ promoted CO oxidation (b) at 98 °C. (c) The $C^{16}O_2$ to $C^{16}O^{18}O$ ratio in the $H_2{}^{18}O$-promoted CO oxidation at the temperature range of 30−105 °C.

Our finding is in sharp contrast to the results of isotopic-labeling experiments in the L−H type reaction over Al_2O_3- and TiO_2-supported Au nanoparticle catalysts in literature.[24,25] In these studies, no incorporation of oxygen from water in the CO_2 product was observed in the H_2O promoted CO oxidation. Instead, water assisted mainly adsorption and/or activation of O_2 molecules.[19−23] In present work, dissociation and desorption of water on ceria are both facile,[40] which are essential for the promotion of water in the MvK type CO oxidation and responsible explicitly for about half amount of CO_2 formation.

In conclusion, a single-atom Pt_1/CeO_2 catalyst was successfully synthesized using ALD technique. In CO oxidation, water showed a remarkable promotion of the activity of Pt_1/CeO_2 catalyst. Our DFT calculations revealed that water affects profoundly the reaction process by opening a new reaction channel for CO oxidation with a lower reaction barrier. Therein, water assists the reaction of CO at Pt_1-top with the hydroxyl group from dissociated water at Ce-top to yield a carboxyl intermediate, and this intermediate dehydrogenated with help of a lattice hydroxyl group to generate CO_2 and water. The overall process is more facile than the direct reaction of CO with the lattice oxygen, resulting in higher activity for CO oxidation. Another important finding is that water directly participates in the CO oxidation, responsible explicitly for about half the amount of the final CO_2 formation, clearly distinct from the water-mediated L−H-type reaction. To the best of our knowledge, this is the first combined experimental and theoretical study of the water-mediated MvK type of CO oxidation. The different roles of water in the water-mediated MvK and L−H reactions might be likely general. Because water is commonly present in reactant gases, the present finding of its direct participation in formation of the final product as a promoter might be stimulating for other oxidation reactions.

DOI: 10.1021/acscatal.6b02685
ACS Catal. 2017, 7, 887−891

■ ASSOCIATED CONTENT

Supporting Information

The Supporting Information is available free of charge on the ACS Publications website at DOI: 10.1021/acscatal.6b02685.

Experimental section, calculation methods, and additional catalytic performance evaluations (PDF)

■ AUTHOR INFORMATION

Corresponding Authors

*E-mail: wxli70@ustc.edu.cn.
*E-mail: junling@ustc.edu.cn.

ORCID

Wei-Xue Li: 0000-0002-5043-3088
Junling Lu: 0000-0002-2607-6869

Author Contributions

‖These authors contributed equally to this work (C.W. and X.-K.G.).

Notes

The authors declare no competing financial interest.

■ ACKNOWLEDGMENTS

This work is supported by the One Thousand Young Talents Program under the Recruitment Program of Global Experts, the NSFC (21473169, 51402283, 21321002, 21225315, and 91645202), the MOST (2013CB834603), the CAS Hundred Talent Program, the Hefei Science Center CAS (2015HSC-UP009), the Fundamental Research Funds for the Central Universities (WK2060030017 and WK2060190026), and the startup funds from University of Science and Technology of China.

■ REFERENCES

(1) Guo, Z.; Liu, B.; Zhang, Q.; Deng, W.; Wang, Y.; Yang, Y. *Chem. Soc. Rev.* **2014**, *43*, 3480−524.
(2) Fu, Q.; Saltsburg, H.; Flytzani-Stephanopoulos, M. *Science* **2003**, *301*, 935−938.
(3) Akiya, N.; Savage, P. E. *Chem. Rev.* **2002**, *102*, 2725−2750.
(4) Cortright, R. D.; Davda, R. R.; Dumesic, J. A. *Nature* **2002**, *418*, 964−967.
(5) Haryanto, A.; Fernando, S.; Murali, N.; Adhikari, S. *Energy Fuels* **2005**, *19*, 2098−2106.
(6) Zope, B. N.; Hibbitts, D. D.; Neurock, M.; Davis, R. J. *Science* **2010**, *330*, 74−78.
(7) Costello, C. K.; Yang, J. H.; Law, H. Y.; Wang, Y.; Lin, J. N.; Marks, L. D.; Kung, M. C.; Kung, H. H. *Appl. Catal., A* **2003**, *243*, 15−24.
(8) Date, M.; Haruta, M. *J. Catal.* **2001**, *201*, 221−224.
(9) Fujitani, T.; Nakamura, I. *Angew. Chem., Int. Ed.* **2011**, *50*, 10144−7.
(10) Ojeda, M.; Iglesia, E. *Chem. Commun.* **2009**, 352−354.
(11) Chang, C. R.; Yang, X. F.; Long, B.; Li, J. *ACS Catal.* **2013**, *3*, 1693−1699.
(12) Mhadeshwar, A. B.; Vlachos, D. G. *J. Phys. Chem. B* **2004**, *108*, 15246−15258.
(13) Gu, X. K.; Ouyang, R. H.; Sun, D. P.; Su, H. Y.; Li, W. X. *ChemSusChem* **2012**, *5*, 871−878.
(14) Gong, X. Q.; Hu, P.; Raval, R. *J. Chem. Phys.* **2003**, *119*, 6324−6334.
(15) Xie, X. W.; Li, Y.; Liu, Z. Q.; Haruta, M.; Shen, W. J. *Nature* **2009**, *458*, 746−749.
(16) Dalai, A. K.; Davis, B. H. *Appl. Catal., A* **2008**, *348*, 1−15.
(17) Kikuchi, R.; Maeda, S.; Sasaki, K.; Wennerstrom, S.; Eguchi, K. *Appl. Catal., A* **2002**, *232*, 23−28.
(18) Date, M.; Okumura, M.; Tsubota, S.; Haruta, M. *Angew. Chem., Int. Ed.* **2004**, *43*, 2129−2132.
(19) Bongiorno, A.; Landman, U. *Phys. Rev. Lett.* **2005**, *95*, 106102.
(20) Saavedra, J.; Doan, H. A.; Pursell, C. J.; Grabow, L. C.; Chandler, B. D. *Science* **2014**, *345*, 1599−1602.
(21) Su, H. Y.; Yang, M. M.; Bao, X. H.; Li, W. X. *J. Phys. Chem. C* **2008**, *112*, 17303−17310.
(22) Liu, L. M.; McAllister, B.; Ye, H. Q.; Hu, P. *J. Am. Chem. Soc.* **2006**, *128*, 4017−4022.
(23) Shang, C.; Liu, Z. P. *J. Phys. Chem. C* **2010**, *114*, 16989−16995.
(24) Calla, J. T.; Davis, R. J. *J. Catal.* **2006**, *241*, 407−416.
(25) Boccuzzi, F.; Chiorino, A.; Manzoli, M.; Lu, P.; Akita, T.; Ichikawa, S.; Haruta, M. *J. Catal.* **2001**, *202*, 256−267.
(26) Lu, J. L.; Elam, J. W.; Stair, P. C. *Surf. Sci. Rep.* **2016**, *71*, 410−472.
(27) Yan, H.; Cheng, H.; Yi, H.; Lin, Y.; Yao, T.; Wang, C. L.; Li, J. J.; Wei, S. Q.; Lu, J. L. *J. Am. Chem. Soc.* **2015**, *137*, 10484−10487.
(28) Sun, S. H.; Zhang, G. X.; Gauquelin, N.; Chen, N.; Zhou, J. G.; Yang, S. L.; Chen, W. F.; Meng, X. B.; Geng, D. S.; Banis, M. N.; Li, R. Y.; Ye, S. Y.; Knights, S.; Botton, G. A.; Sham, T. K.; Sun, X. L. *Sci. Rep.* **2013**, *3*, 1775.
(29) Ding, K.; Gulec, A.; Johnson, A. M.; Schweitzer, N. M.; Stucky, G. D.; Marks, L. D.; Stair, P. C. *Science* **2015**, *350*, 189−192.
(30) Qiao, B. T.; Wang, A. Q.; Yang, X. F.; Allard, L. F.; Jiang, Z.; Cui, Y. T.; Liu, J. Y.; Li, J.; Zhang, T. *Nat. Chem.* **2011**, *3*, 634−641.
(31) Aleksandrov, H. A.; Neyman, K. M.; Hadjiivanov, K. I.; Vayssilov, G. N. *Phys. Chem. Chem. Phys.* **2016**, *18*, 22108−22121.
(32) Bera, P.; Gayen, A.; Hegde, M. S.; Lalla, N. P.; Spadaro, L.; Frusteri, F.; Arena, F. *J. Phys. Chem. B* **2003**, *107*, 6122−6130.
(33) Bruix, A.; Lykhach, Y.; Matolinova, I.; Neitzel, A.; Skala, T.; Tsud, N.; Vorokhta, M.; Stetsovych, V.; Sevcikova, K.; Myslivecek, J.; Fiala, R.; Vaclavu, M.; Prince, K. C.; Bruyere, S.; Potin, V.; Illas, F.; Matolin, V.; Libuda, J.; Neyman, K. M. *Angew. Chem., Int. Ed.* **2014**, *53*, 10525−10530.
(34) Peterson, E. J.; Delariva, A. T.; Lin, S.; Johnson, R. S.; Guo, H.; Miller, J. T.; Kwak, J. H.; Peden, C. H. F.; Kiefer, B.; Allard, L. F.; Ribeiro, F. H.; Datye, A. K. *Nat. Commun.* **2014**, *5*, Article No. 4885.
(35) Yang, X. F.; Wang, A. Q.; Qiao, B. T.; Li, J.; Liu, J. Y.; Zhang, T. *Acc. Chem. Res.* **2013**, *46*, 1740−1748.
(36) Vile, G.; Albani, D.; Nachtegaal, M.; Chen, Z. P.; Dontsova, D.; Antonietti, M.; Lopez, N.; Perez-Ramirez, J. *Angew. Chem., Int. Ed.* **2015**, *54*, 11265−11269.
(37) Mars, P.; van Krevelen, D. W. *Chem. Eng. Sci.* **1954**, *3*, 41−59.
(38) Doornkamp, C.; Ponec, V. *J. Mol. Catal. A: Chem.* **2000**, *162*, 19−32.
(39) Lykhach, Y.; Johanek, V.; Aleksandrov, H. A.; Kozlov, S. M.; Happel, M.; Skala, T.; St Petkov, P.; Tsud, N.; Vayssilov, G. N.; Prince, K. C.; Neyman, K. M.; Matolin, V.; Libuda, J. *J. Phys. Chem. C* **2012**, *116*, 12103−12113.
(40) Mullins, D. R.; Albrecht, P. M.; Chen, T. L.; Calaza, F. C.; Biegalski, M. D.; Christen, H. M.; Overbury, S. H. *J. Phys. Chem. C* **2012**, *116*, 19419−19428.
(41) Wang, Y. G.; Mei, D. H.; Li, J.; Rousseau, R. *J. Phys. Chem. C* **2013**, *117*, 23082−23089.

DOI: 10.1021/acscatal.6b02685
ACS Catal. 2017, 7, 887−891